Chapter 11
Materials for Organic Light Emitting Diode (OLED)

Takashi Karatsu

11.1 OLED and Phosphorescent Cyclometalated Iridium (III) Complexes

Iridium complexes have a wide range of applications such as photocatalysts to reduce carbon dioxide [1], imaging reagents for living cells [2], and oxygen sensors [3]. In particular, organic light emitting diodes (OLED) is one of important industrial application for iridium complexes, due to their high phosphorescent efficiency at ambient temperature [4, 5]. OLEDs have many advantages, including self-emission (no backlight required), an almost 180° wide view angle, light weight, thin (<2 mm), quick response (1,000 times faster than LCD), high contrast, and can be fabricated on flexible plastic substrates.

In 1987, Tan et al. reported the potential of OLEDs using tris (8-hydroxyquinolinato) aluminium (III) (Alq_3) [6]. Before them, the OLED device has simple configuration that has single organic crystal sandwiched by two electrodes. They introduced concept of OLED device configuration composed of multiple thin layers (Fig. 11.1). Here, each layer has an exact function, such as charge transporting and emitting abilities. The external efficiency of this OLED device was 1 %, which meant an internal efficiency of 5 %, because the output efficiency from the device was approximately 20 % [7]. After charge (hole and electron) injection into the emitting layer, 25 % singlet and 75 % triplet excitons are generated by charge recombination. Therefore, the only usable amount of fluorescence is 25 %. If phosphorescent materials can be used, then the 75 % triplet excitons are usable. In addition, the triplet excited state has lower energy than the singlet excited state; therefore, there is a chance that intersystem crossing of singlet excited state to the triplet excited state could occur.

T. Karatsu (✉)

Department of Applied Chemistry and Biotechnology, Graduate School of Engineering,
Chiba University, 1-33, Inage-ku, Chiba 263-8522, Japan
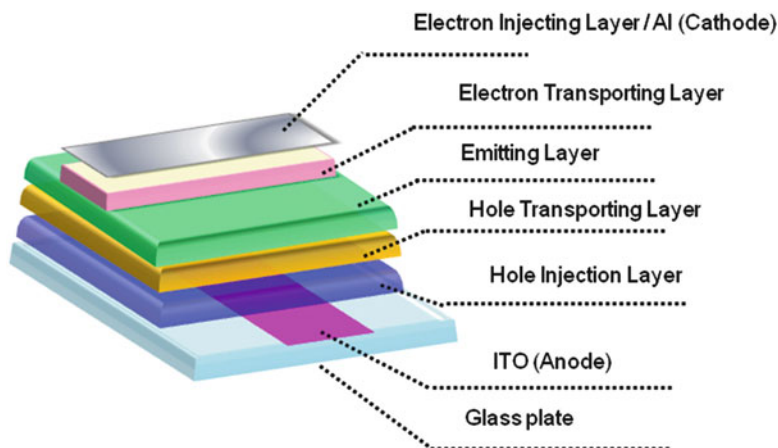e-mail: karatsu@faculty.chiba-u.jp

Fig. 11.1 Configuration of OLED device composed of multiple thin layers

In 1998, Thompson and co-workers reported a device that employed 2,3,7,8,12,13,17,18-octaethyl-12*H*,23*H*-porphine platinum(II) (PtOEP), which had an external quantum efficiency of 4 % [8, 9]. In 1999, the efficiency of PHOLED was improved to 7.5 % using phosphorescent *fac*-tris (2-phenylpyridinato,$NC^{2'}$)iridium(III) (*fac*-Ir(ppy)$_3$) [10, 11]. These reports boosted the research activity in this field. The efficiency was jumped up to 29 %, using also *fac*-Ir(ppy)$_3$, as reported by Kido and co-workers in 2007 [5]. This meant internal emission quantum efficiency reached 100 %. Here, not only triplet excitons (75 %), but also singlet excitons (25 % singlet excitons also generate triplet excitons after intersystem crossing) were used after charge recombination. Phosphorescent triscyclometalated iridium complexes have advantage to obtain wide variety of the emission colors by changing structure of cyclometalated ligands.

Recent development of OLED materials has been focused on the maximizing substance ability to each function, such as charge injection and transport ability, emitting ability, exciton confinement ability, and so on. Designing of the materials has wide varieties based on variation of organic molecules. In this chapter, it is focused on the materials forming the emitting layer, especially, the nature of phosphorescent triscyclometalated iridium (III) complexes. Selection of cyclometalated ligands from the wide variation of organic molecules provides fine tuning of phosphorescence color. The typical triscyclometalated iridium (III) complexes consist of three bidentate ligands to make octahedral structure surrounding iridium atom, and symmetry generated by these coordination provides *fac* and *mer* geometrical isomers. Each isomer has *Δ* and *Λ* optical isomers. Their selective preparation and characteristic in the excited state including isomerization between their isomers are the main part in the next section [12–14]. In addition, comparing with blue, green, and red phosphorescent complexes, blue phosphorescent complexes have difficulties for their emission color purities and materials stabilities. Therefore, one section is spent to explain recent development of blue

phosphorescent iridium complexes [15, 16]. Iridium complexes have been used as dopant in an emitting layer, therefore, host materials are also important. Host materials require high abilities of charge transport and confinement of triplet energy of dopant exciton. In the last part, our attempt to develop wet processable host materials for green to blue phosphorescent complexes has been mentioned. Wet process is one of the key processes to reduce process cost and improve quality of large area devices by climbing over difficulties of vacuum sublimation method [17–19].

11.2 *Meridional* and *Facial* Isomers of Iridium Complexes and Their Photochemical Isomerization

Ir(ppy)$_3$, (tris(4,6-difluorophenyl)pyridinato,$NC^{2'}$) iridium (III) (Ir(F$_2$ppy)$_3$), and other triscyclometalated iridium (III) complexes have d^6 electron configuration, and have octahedral structure (Fig. 11.2). Ir(ppy)$_3$ has three 2-phenylpyridine bidentate ligands and coordinated at 2-phenyl anionic carbon and pyridyl nitrogen atoms. This is quite different from nitorogen atom coordinated ruthenium (II) trisbipyridine (Ru(bpy)$_3$). Symmetry generated C and N atom coordinations makes *fac* and *mer* isomers. Here in the *fac*-isomer, three pyridyl nitrogen atoms locate vertexes of a triangle make up of octahedron. On the other hand, three pyridyl nitrogen atoms locate on the meridian of *mer*-isomer. Up-to-date, photophysics and photochemistry of the *fac*-isomer have been caught attention and studied extensively, however, those of the *mer*-isomer have been caught limited attention. The reasons are synthetic easiness, chemical stability, and high emission ability of the *fac*-isomer. In addition, each *fac*- and *mer*-isomer has Δ- and Λ − optical isomers, and those characteristics have also been studied minimal. In this section, characters of those isomers and photochemical isomerization between those isomers are described. Radiative process is important as a radiative material, however, understanding of nonradiative process that is a complemental process to
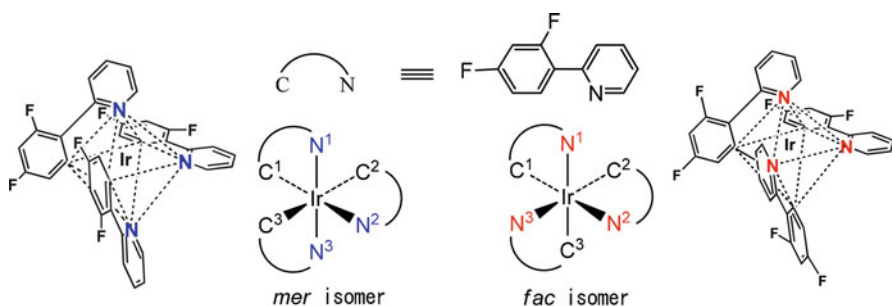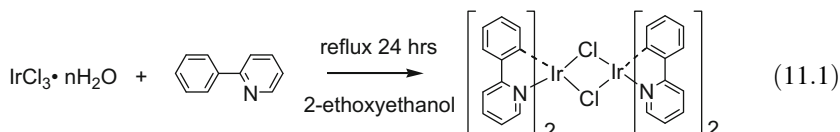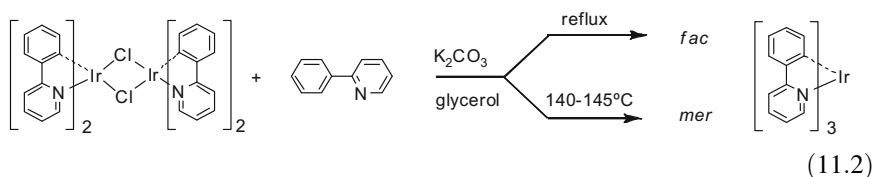

Fig. 11.2 Structures of *mer* and *fac* isomers of Ir(F$_2$ppy)$_3$, and their abbreviated structures

the radiative process is also important for the understanding of radiative materials and chemical stability of the materials.

For syntheses of the iridium complexes, Nonoyama method through Ir(III) chlorine μ dimer complex is widely used (Eq. (11.1)) [20]. For this reaction and following reaction introducing the third ligand are typically quantitative and are performable under a moderate reaction condition. R. J. Watts and co-workers reported 10 % formation of Ir(ppy)$_3$ beside formation of Cl-μ dimer complex [21].

$$IrCl_3 \cdot nH_2O \ + \quad \text{[2-phenylpyridine]} \quad \xrightarrow[\text{2-ethoxyethanol}]{\text{reflux 24 hrs}} \quad \text{[Cl-bridged Ir dimer complex]} \tag{11.1}$$

The reaction yield from μ-dimer complex was improved by using silver triflate (trifluoromethanesulfonate) as using leaving group and also dechlorination reagent [22]. The synthesis of the triscyclometalated complex has been reported to synthesize by one-step reaction from tris(acetylacetonato) Ir(III) complex [23]. For the preparation and purification methods for *mer*-isomer have not been well studied and have not established. Recently, selective preparation method of the *fac*- and *mer*-isomer has been reported by controlling reaction temperature. The *mer*-isomer has been prepared 65–80 % reaction yield under mild condition in the presence of base at ambient temperature to 150 °C [24, 25] (Eq. (11.2)). In addition, a method through bis(phenylpyridinato)acetylacetonato iridium (III) complex synthesized from μ-dimer complex, and then acetylacetonato ligand was converted to the third ligand improves reaction yield of the *mer*-isomer [12]. In general, reaction under the mild condition gives *fac-mer* mixture, and [*mer*]/[*fac*] ratio is increased and total reaction yield is decreased by decreasing reaction temperature. Ligands exchange reaction proceeds through thermodynamic controlled mechanism giving thermodynamic stable *fac*-isomer as a product at high temperature, and kinetic favored *mer*-isomer is produced at ambient temperature. Usually, *fac*-isomer is almost 10 kcal mol^{-1} more stable than the corresponding *mer*-isomer [13].

$$\text{[Cl-bridged Ir dimer complex]} \ + \ \text{[2-phenylpyridine]} \quad \xrightarrow[\text{glycerol}]{K_2CO_3} \quad \begin{matrix} \xrightarrow{\text{reflux}} & fac \\ \xrightarrow{140\text{-}145°C} & mer \end{matrix} \quad \text{[Ir complex]}_3 \tag{11.2}$$

For the synthesis expressed in Eq. (11.2), glycerin used as typical solvent even hard to reach its boiling point. In such case, use of microwave reactor is useful method, and this shortened reaction time. On the other hand, synthesis for heat sensitive complexes, decomposition of the complex becomes problem. In such cases, use of *mer* → *fac* photochemical isomerization after the synthesis of the *mer*-isomer is very useful method [22, 23].
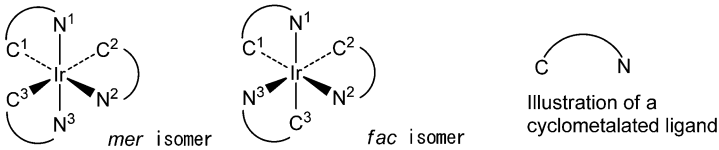
The isomers were separated by a column chromatography and purified by the crystallization, and analyzed by HPLC, NMR, elemental analysis, X-ray crystallography. Especially, by means of H NMR, signals from three ligands are appeared in equivalent for the *fac*-isomers, but inequivalent for *mer*-isomers. For ^{13}C NMR, signals of the *mer*-isomer's are triple than those of the *fac*-isomer's.

There are some reports for structures of the complexes by a single crystal X-ray crystallography. All of the crystals were racemic crystal consist of 1:1 Δ- and Λ-enantiomers. There have been reported many data for the *fac*-isomers [13, 24], and not so many for the *mer*-isomers [12, 24]. Therefore, there are limited cases we can compare those structures. The *fac*-isomers have higher symmetry than the *mer*-isomers. All of *trans* positions of Ir–N bond are Ir–C bonds for *fac*-isomer. On the other hand, combination of the atoms of *trans* positions of the *mer*-isomer are N–Ir–N, N–Ir–C, and C–Ir–C. These bond lengths reported for tris(1-phenylpyrazolato, $NC^{2'}$)iridium(III) (Ir(ppz)$_3$) are compared between *fac*- and *mer*-isomers (Table 11.1). In case of the *fac*-isomer, bond lengths of three pairs of Ir–C and Ir–N bonds are almost same. Mean values of Ir–C and Ir–N bond lengths are 2.02 and 2.12 Å, respectively, and always Ir–N bonds are longer than Ir–C bonds. On the other hand, for the *mer*-isomer, bond length has a large variation, and difference in bond length of Ir–N and Ir–C is small. Relation Ir–N > Ir–C accomplished in the *fac*-isomer, does not hold in the *mer*-isomer. Bond lengths of Ir–C^2 and Ir–C^3, those are in *trans* position each other, are long and similar *trans* position of Ir–N^1 and Ir–N^3 bond lengths are short. This kind of relation in bond length is generally found for other iridium (III) complexes (Table 11.1).

Measurments of the absorption spectra and emission spectra gave excitation energies, emission lifetimes (τ_p) and emission quantum yields (Φ_p) and then radiative rate constant ($k_r = \Phi_p/\tau_p$) and nonradiative rate constant ($k_{nr} = (1-\Phi_p)/\tau_p$) as shown in Table 11.2. For example, absorption spectrum of *fac*-Ir(F$_2$ppy)$_3$ is very similar to that of *fac*-Ir(ppy)$_3$ [21, 26–29], however, spectrum of *mer*-Ir(F$_2$ppy)$_3$ was quite different from the following two points. In the short wavelength region, π–π* absorption band splitted to two bands for *fac*-isomer was single in the case of *mer*-isomer, and decrease of molar extinction coefficient was observed for [1]MLCT band around 350 nm. Phosphorescence band of the *mer*-isomer generally appeared at longer wavelengths than that of the corresponding *fac*-isomer, and degree of shift is between a couple of nanometers and up to 50 nm dependent on the ligand. Φ_p values of *mer*-isomer were extremely smaller than that of *fac*-isomer. Emission lifetime of *mer*-isomer measured by a single photon counting method was shorter than that of the *fac*-isomer. As a result, no significant difference between k_r of *mer*- and *fac*-isomers and difference in Φ_p and τ_p was caused by difference of k_{nr}.

The significantly low ability of phosphorescence of *mer*-isomer was partly due to the photochemical isomerization. Irradiation of UV light induced *mer* → *fac* isomerization under deaerated solution, and emission spectrum and lifetime were identical with those of the *fac*-isomer, and product was finally identified as the *fac*-isomer by chemical analytic methods such as ^{1}H NMR and mass spectrometry. On the other hand, irradiation of the *fac*-isomer brought no chemical change at the same reaction condition. This means this isomerization is *mer* → *fac* one-way (Fig. 11.3).

Table 11.1 Key bond lengths and bond angles of *mer* and *fac* isomers obtained by single-crystal X-ray diffraction method

Illustration of a cyclometalated ligand

Bond length (Å) or angle (°)	Ir(ppz)$_3$		Ir(CF$_3$ppz)$_3$		Ir(F$_2$ppy)$_3$	
	mer	*fac*	*mer*[a]	*fac*[a]	*mer*	*fac*
Ir–N^1 (Å)	2.013	2.135	2.016	2.113	2.018	2.118
Ir–N^2	2.049	2.121	2.104	2.111	2.142	2.128
Ir–N^3	2.025	2.118	2.014	2.108	2.041	2.116
Ir–C^1 (Å)	1.994	2.027	1.999	2.017	2.030	2.011
Ir–C^2	2.061	2.021	2.078	2.014	2.077	2.002
Ir–C^3	2.053	2.016	2.078	2.019	2.067	1.997
N^1–Ir–C^1 (°)	79.63	79.50	80.32	79.02	81.12	79.32
N^2–Ir–C^2	79.13	79.62	78.27	79.26	78.69	79.47
N^3–Ir–C^3	78.49	78.73	79.13	79.19	80.32	79.33
N^1–Ir–N^3 (°)	171.52		172.25		173.24	
C^1–Ir–N^2	172.17		170.18		175.30	
C^2–Ir–C^3	172.68		169.62		172.60	
N^1–Ir–C^3 (°)		170.56		170.93		172.50
N^2–Ir–C^1		170.05		169.57		174.16
N^3–Ir–C^2		171.32		168.60		170.41

[a]Average of Δ and Λ isomers

Table 11.2 Phosphorescence quantum yields (Φ_p), lifetime (τ), radiative (k_r) and nonradiative rate constants (k_{nr}) of iridium (III) triscyclometalate complexes [12, 13, 24]

Complex	Φ_p	τ/µs	k_r/s^{-1}	k_{nr}/s^{-1}
fac-Ir(ppy)$_3$ [24]	0.4	1.9	2.1×10^5	3.2×10^5
mer-Ir(ppy)$_3$ [24]	0.036	0.15	2.4×10^5	6.4×10^6
fac-Ir(tpy)$_3$ [24]	0.5	2	2.5×10^5	2.5×10^5
mer-Ir(tpy)$_3$ [24]	0.051	0.26	2.0×10^5	3.6×10^6
fac-Ir(F$_2$ppy)$_3$ [12]	0.43	1.6	2.7×10^5	3.6×10^5
mer-Ir(F$_2$ppy)$_3$ [12]	0.053	0.21	2.5×10^5	4.5×10^6
fac-Ir(ppz)$_3$[a][13]	1	28	3.3×10^4	3.3×10^6
mer-Ir(ppz)$_3$[a][13]	0.81	14	6.4×10^4	6.4×10^6
fac-Ir(tpy)$_2$(ppz) [13]	0.35	1.5	2.3×10^5	4.1×10^5
mer-Ir(tpy)$_2$(ppz) [13]	0.012	0.064	1.9×10^5	1.5×10^7
fac-Ir(tpy)(ppz)$_2$ [13]	0.37	1.8	2.1×10^5	3.6×10^5
mer-Ir(tpy)(ppz)$_2$ [13]	0.068	0.4	1.7×10^5	2.5×10^6

[a]Rate constants, k_{nr} is estimated on the assumption that k_r at 77 K and that at ambient temperature are equal, because those complexes did not give phosphorescence at ambient temperature in solution
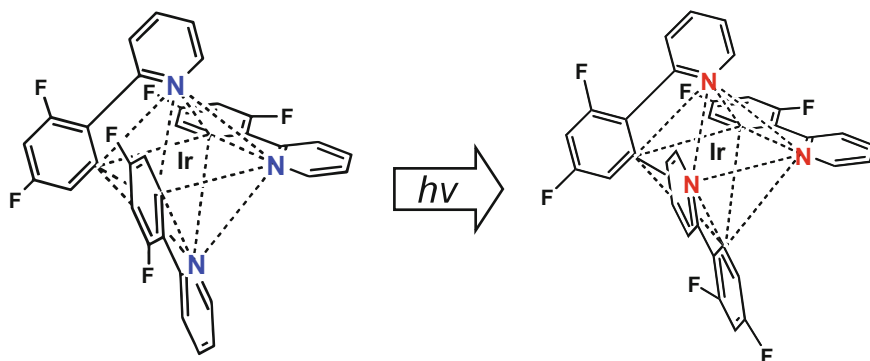
Fig. 11.3 Photochemical *mer* → *fac* one-way isomerization of Ir(F$_2$ppy)$_3$ complex

Table 11.3 Quantum yield of photochemical *mer* → *fac* isomerization (Φ_{isom}) in deaerated solution (CH$_3$CN)

Complex	Φ_{isom}
mer-Ir(F$_2$ppy)$_3$	0.067
mer-Ir(tpy)$_3$	0.00018
mer-Ir(tpy)$_2$(ppz)	0.00028
mer-Ir(tpy)(ppz)$_2$	0.12
mer-Ir(ppz)$_3$	0.072

Photochemical *mer* → *fac* one-way isomerization quantum yield were between 0.12 and 10^{-4} in deaerated acetonitrile at ambient temperature as shown in Table 11.3 [12, 13]. An activation energy of this isomerization was determined to be 15.2 kJ mol^{-1} by the Arrhenius plot of the isomerization rate constants for Ir (F$_2$ppy)$_3$. Both emission and isomerization were quenched by the triplet quencher azulene that has lowest triplet energy $E_T = 163$ kJ mol^{-1}. This indicated that the emission was phosphorescence and the isomerization also occurred via a triplet excited state. Φ_{isom} values showed quite small <0.1 quantum yield in the temperature range between 283 and 313 K. On the other hand, temperature dependence of Φ_P showed large dependence on temperature, and Φ_P increased intensity by decreasing measurement temperature. At temperature $T \leqq 243$ K, *mer*-isomer showed equivalent to the *fac*-isomer's Φ_P at ambient temperature. Therefore, the isomerization and phosphorescence do not act as complementally that indicates the isomerization do not occurred through ^{3}MLCT state (phosphorescent state).

This isomerization require activation energy. The reaction quantum yields (Φ_{react}) decreases by decreasing reaction temperature. Comparing temperature dependence of isomerization of *mer*-Ir(F$_2$ppy)$_3$ [12] and carbonyl ligand and solvent acetonitrile exchange reaction of renium carbonyl complex showed similarity [30]. Emission quantum yields (Φ_{em}) and Φ_{react} behave complementary, therefore, Φ_{em} are increasing by decreasing temperature, however, Φ_{react} are decreasing by decreasing temperature. For the exchange reaction, $\Phi_{\text{react}} + \Phi_{\text{em}}$ was almost constant in the measured temperature range, however, $\Phi_{\text{react}} + \Phi_{\text{em}}$
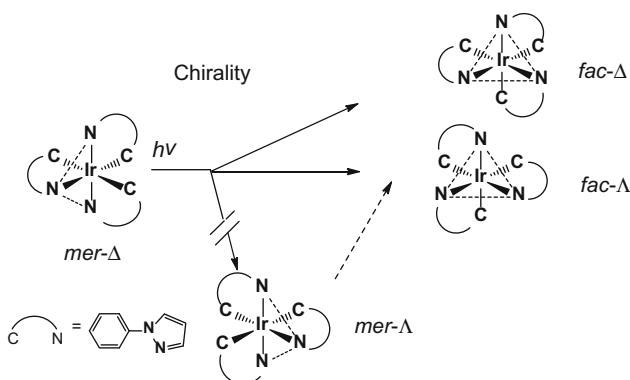
Fig. 11.4 Chirality in the photochemical isomerization of *mer-Δ*-Ir(ppz)$_3$ in solution. This reaction produced no *mer-Λ* isomer, but *fac-Δ* and *-Λ* isomers. The *fac-Δ* isomer was produced in excess amount

was not constant for the isomerization implying existence of another deactivation path. From the above results, a plausible reaction mechanism is proposed as follows. This isomerization occurs through thermally accessible ^{3}d* state, which is in equilibrium between emissive ^{3}MLCT state.

Ir(ppz)$_3$ complex is interesting because this complex is not only *mer*-isomer but also *fac*-isomer also does not give phosphorescence at ambient temperature in solution. Reason of these phenomena must be *mer → fac* one-way isomerization or enantiomeric isomerization between *Δ*- and *Λ*-isomers through a twist mechanism or ligand dissociation-association mechanism. We optical resolved *Δ*- and *Λ*-isomers of Ir(ppz)$_3$, and examined their photochemical isomerization (Fig. 11.4) [14].

Through the twist mechanism of both *mer* and *fac* isomers cause no *mer-fac* geometrical isomerization but only cause *Δ − Λ* optical isomerization. *Mer* and *fac* isomers cause optical isomerization and geometrical isomerization by dissociation-recoordination mechanism. For example, irradiation of *mer-Δ* isomer of Ir(ppz)$_3$ produced *fac-Δ* and *fac-Λ* isomers, however, no production of the *mer-Λ* isomer (Fig. 11.4). Here, *fac-Δ* and *Λ* isomers were produced 59 and 41 %, respectively. This means *fac-*Δ isomer is produced in 18%ee (enantio excess). Plausible reaction mechanism is trigonal bipyramidal (TBP) mechanism as shown in Fig. 11.5.

There are two important points to consider this isomerization mechanism. The first point is identification of photochemically active ligand, here, there is Adamson's empirical rule [31–36]. There is argument for the application limit of this rule, however, photochemistry of iridium complexes fits very well. According to this rule, individual Ir–N bond in axial position dissociates of *mer-Δ* isomer, Ir–N^1 bond dissociation (Route A) gives *fac-Δ* isomer (chirality retains) and Ir–N^3 bond dissociation (Route B) gives *fac-Λ* (chirality inversion) isomer. The second point is that C–Ir–N axis (not C–Ir–C axis) is kept in two diastereomeric TBP intermediates. If these two hypothesis hold in the mechanism, we can rationally explain experimental results. Reason why enantio-excess arise is explained by the different efficiency over come diastereomeric transition states (Fig. 11.6).
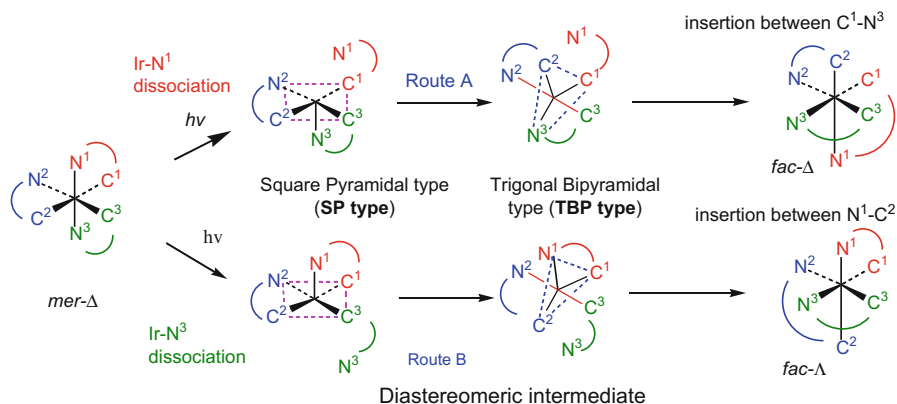
Fig. 11.5 Isomerization mechanism through dissociation and recoordination (TBP mechanism)

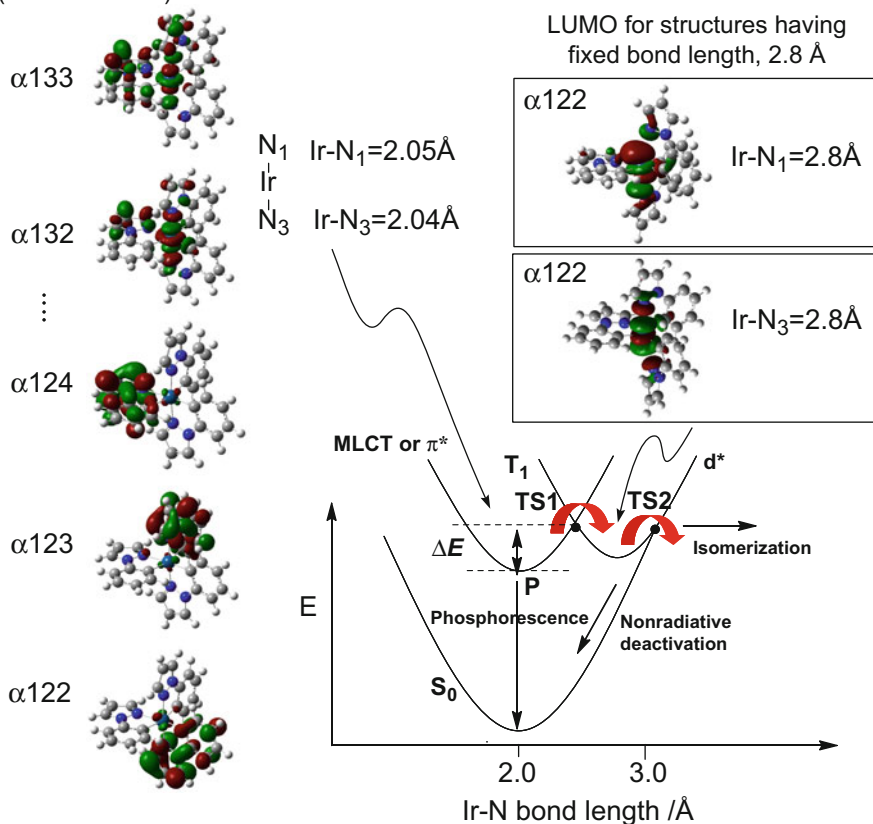MO for optimized structure
(LUMO is α122)

Fig. 11.6 Potential energy surfaces of ground state and excited state and their MO

Lowest triplet excited state generated by the excitation gives ^{3}MLCT state. Structures for this state, elongation of Ir–N^1 or Ir–N^3 bond gives d* state through the transition state caused by energy surface crossing (TS1). In this structure, axial bond shows anti-bonding nature. Difference in activation energies (ΔE_a) formed by bond elongation of Ir–N^1 or Ir–N^3 determines enantioexcess value.

Whether this isomerization occurs or not in solid phase, *fac*- and *mer*-Ir(ppy)$_3$ gave equivalent PL efficiency in EPA at 77 K, and PL lifetimes were 2.83 and 2.65 μs for *mer*- and *fac*-isomer, respectively. In addition, relative PL intensities of powder *mer*- and *fac*-isomer were equivalent. Therefore, isomerization is not important, however, there is a chance that this isomerization may take place during vacuum sublimation process.

OLED device composed of *mer*-Ir(ppy)$_3$ gave equivalent efficiency as a device of *fac*-isomer [37]. Actually, radiative rate constants of the *mer*-isomers are almost identical with those of the corresponding *fac*-isomer, this is quite reasonable considering that molecular motion and structural transformation are prohibited in the solid state device. On the other hand, efficiency of the emission decreased for the device composed of *fac*-isomer doped with small amount of the *mer*-isomer. This is explained by the trapping of the excitation energy at *mer*-isomers. *Mer*-isomer which has smaller excitation energy than that of the *fac*-isomer acts as a trap site. In addition, *mer*-isomer may have smaller emission efficiency than corresponding *fac*-isomer [38]. PL of *fac*-Ir(ppy)$_3$ doped in CBP, in the case of no *mer*-isomer doped, i.e. [*mer*-isomer] = 0 %, Φ_{PL} was 92 %, and this value decreased to 48 and 37 % when doped *mer*-isomer concentrations were 30 and 46 %, respectively.

This *mer* → *fac* one-way isomerization is often observed for blue phosphorescent Ir(III) complexes, since energy level of phosphorescent state is high and it locates nearby d* state that is responsible for the isomerization [12–14]. However, recent our report showed that no *mer* → *fac* isomerization occurred for blue phosphorescent Ir(III) complexes having carbene type ligand such as tris[2-(4-X-phenyl)-3-butyl-[1,3]-imidazolinato-C^2, N^1]iridium (III) X=fluoro, *mer*-Ir(Fpim)$_3$; X=trifuluoromethyl, *mer*-Ir(CF$_3$pim)$_3$; and X=trifluoromethoxy, *mer*-Ir(OCF$_3$pim)$_3$ [15].

11.3 Blue Phosphorescent Cyclometalated Iridium (III) Complexes and Their Nonradiative Deactivation

For PHOLED, red and green phosphorescent iridium complexes have been used in commercial devices [39]. However, compared to the significant success of green and red phosphorescent materials, there are still difficulties with blue phosphorescent materials, which is the barrier to achieve total phosphorescent full color display and white color lighting.
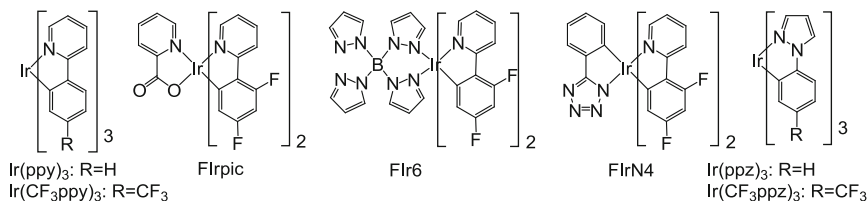
Fig. 11.7 Typical blue phosphorescent Ir (III) complexes

There are three difficulties with blue Phosphorescent OLEDs. The first is that they do not have sufficient color purity. The National Television Standards Committee (NTSC) determined that the Commission Internationale de l'Eclairage (CIE) coordinates for blue are (x, y = 0.14, 0.08). However, in typical blue phosphorescent complexes, such as iridium (III) bis(4,6-difluorophenylpyridinato)picolinate (FIrpic) [40], iridium (III) bis(4,6-difluorophenylpyridinato)tetrakis(1-pyrazolyl) borate (FIr6) [41], and iridium (III) bis(4,6-di-fluorophenylpyridinato)-5-(pyridine-2-yl)-1H-tetrazolate (FIrN4) [42], the sum of the x, y coordinates is more than 0.3, and the color is called sky blue. The second difficulty is insufficient emission efficiency (Fig. 11.7). A blue phosphorescent complex has a higher emission state (^{3}MLCT, metal-to-ligand charge-transfer) than other color complexes, due to the large transition energy. This enables thermal activation to the metal-centered excited state (d*), which promotes nonradiative deactivation. For example, *fac*-Ir(ppz)$_3$ has strong blue phosphorescence ($\Phi_{PL} = 1.0$) at 77 K, but has almost no emission at 298 K ($\Phi_{PL} = 0.001$) [24]. This is explained by thermal excitation to the upper ^{3}d* state, which is responsible for nonradiative deactivation from the phosphorescent ^{3}MLCT* state at 298 K [43]. In addition, the development of host and carrier transport materials for blue phosphorescent materials is also very important, because the high triplet excitation energy of blue phosphorescent materials is becoming difficult to confine [40]. This accompanies tuning of the HOMO–LUMO level of the host and carrier transport materials, and causes a decrease of the carrier transport efficiency, which has an influence on device lifetime. For example, a device composed of FIrpic produced a large amount of defluorinated product (detected by mass spectrometry (MS)) after application of voltage–current at 10 V, 100 mA/cm^2 for 24 h [44]. Substitution with the strong electron-withdrawing difluoro group on the phenyl ring is an effective method to decrease the x + y value, and has thus been one of the main methods. However, there may be a shift toward the development of fluorine-free materials [45].

Computational investigation of *fac*-Ir(ppy)$_3$ revealed that the HOMO is mainly localized at the iridium d-orbital and phenyl moiety, and the LUMO is localized at the pyridyl moiety. Therefore, control of the HOMO–LUMO energy gap has been attempted by the modification of green phosphorescent *fac*-Ir(ppy)$_3$ using the following three strategies.

(1) Stabilization of HOMO by the introduction of electron withdrawing groups (EWGs) on a phenyl ring: Thompson and co-workers reported an OLED device
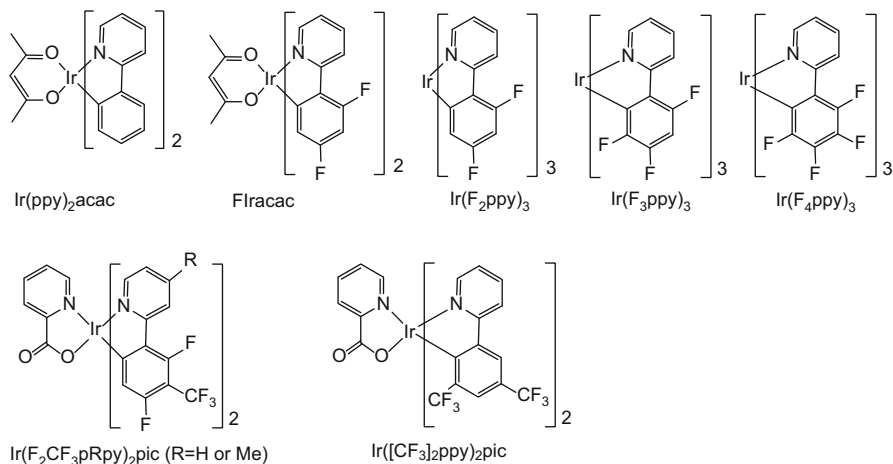
Fig. 11.8 Complexes with electron withdrawing groups

doped with *fac*-Ir(ppy)$_3$ in 1999, and thereafter reported several homoleptic complexes. A typical preparation is conducted through a μ-Cl dimer complex; however, there are difficulties involved. Thompson and co-workers also reported the synthesis and use of a diketonate complex through a dimer complex in 2001 [46]. These diketonate complexes have equivalent or slightly lower emission efficiency than the homoleptic complexes; however, they are easily synthesized. Many green and red phosphorescent diketonate complexes have also been reported [47]. Iridium (III) bis(4,6-difluorophenylpyridinato) acetylacetonate (FIr(acac)) and FIrpic were reported in 2001 (Fig. 11.8) [40]. Both complexes exhibited very high efficiency emission; λ_{max} for FIr(acac) is blue-shifted 40 nm compared with that for iridium (III) bis(2-phenylpyridinato) acetylacetonate (Ir(ppy)$_2$(acac)), and λ_{max} for FIrpic is also blue-shifted 20 nm compared with that for FIr(acac). These results indicate that the introduction of fluoro groups on the phenyl stabilizes the HOMO, because the HOMO is partly localized at the phenyl moiety. In addition, changing the ancillary ligand to the EWG picolinate also stabilized the HOMO partly localized at the d-orbital of the metal center.

Thompson and co-workers also reported *fac*-Ir(F$_2$ppy)$_3$ in 2003 [24]; however, λ_{max} for this complex was the same as FIrpic (468 nm). In 2006, De Cola and co-workers reported a complex with trifluoro groups introduced on the phenyl rings of Ir(ppy)$_3$, *fac*-iridium (III) tris(3,4,6-trifluorophenylpyridinate) (*fac*-Ir(F$_3$ppy)$_3$), in addition to a complex with tetrafluoro groups, *fac*-iridium (III) tris(3,4,5,6-tetrafluorophenylpyridinate) (*fac*-Ir(F$_4$ppy)$_3$). These complexes had λ_{max} at 459 and 468 nm, respectively [48]. Interestingly, the increased number of F substitution, from three to four, resulted in red-shift of λ_{max} (decrease of the HOMO–LUMO energy gap). In the same year, Yamashita and co-workers reported trifluoromethyl substituted FIrpic, iridium
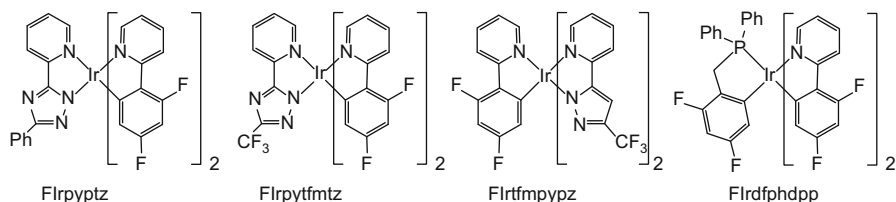
Fig. 11.9 Complexes with electron withdrawing ancillary ligands

(III) bis(2,4-difluoro-3-(trifluoromethyl)phenylpyridinato)picolinate (Ir(F_2CF_3pRpy)$_2$pic), and iridium (III) bis(2,4-difluoro-3-(trifluoromethyl)phenyl-4- methylpyridinato)picolinate, which had λ_{max} at 457 and 454 nm, respectively [49]. Che and co-workers reported λ_{max} for iridium (III) bis(3,5-bis(trifluoromethyl)phenylpyridinato)- picolinate (Ir([CF_3]$_2$ppy)$_2$(pic)) as 471 nm in 2008 [50]. These attempts demonstrate the effectiveness and limitations of design for blue phosphorescent Ir complexes by tuning of the HOMO energy level.

(2) Using strong EWG ancillary ligands: Many types of ancillary ligands have been added to the complexes after FIrpic exhibited a shorter λ_{max} than FIracac. In 2003, Thompson and co-workers reported FIr6 with borate as a ancillary ligand, and this complex had λ_{max} at 457 nm [41]. In 2004, De Cola and co-workers reported iridium (III) bis(4,6-difluorophenylpyridinato)pyridyltriazole with λ_{max} at 461 nm ($\Phi_{PL} = 0.27$) [51]. At this stage, pyridyl-azole type ligands became popular. Chi and co-workers reported in 2005 that iridium (III) bis(4,6-difluorophenylpyridinato)-3-(trifluoromethyl)-5-(pyridine-2-yl)-1,2,4-triazolate and FIrN4 had λ_{max} at 460 and 459 nm, respectively (Fig. 11.9) [46]. Then in 2007, iridium (III) bis(2-pyridyl-3-trifluoromethylpyrazolato)-4,6-difluorophenylpyridinate, which has pyridyltrifluoromethylpyrazole as main ligands, had λ_{max} at 450 nm ($\Phi_{PL} = 0.50$) [52]. Chi and co-workers reported a phosphine type ligand in 2009 [53]; iridium (III) bis(4,6-difluorophenylpyridinato)-(2,4-difluorobenzyl)diphenylphosphinate had λ_{max} at 457 nm ($\Phi_{PL} = 0.19$) [54].

(3) Breakaway from phenyl pyridinato complexes, using phenylheterocycles: Complexes with many types of ancillary ligands have been synthesized; however, the shift of λ_{max} was only 10 nm, and color clarity of the blue was less than satisfactory. Further blue-shift is very difficult using difluorophenylpyridine as a ligand; therefore, an approach to tune the resonance stabilization energy by changing the pyridyl group to other heterocycles was attempted. In 2003, complexes with phenyl pyrazole type ligand were reported [24]. *fac*-Ir(ppz)$_3$ and the 4,6-difluorophenyl derivatives *fac*-Ir(F_2ppz)$_3$ exhibited phosphorescence at 77 K with λ_{max} at 414 and 390 nm, respectively. This was a significant blue-shift compared to phenyl pyridine based complexes such as *fac*-Ir(F_2ppy)$_3$ ($\lambda_{max} = 450$ nm). However, these complexes in solution were poorly phosphorescent at room temperature ($\Phi_{PL} < 0.001$). Thompson and co-workers
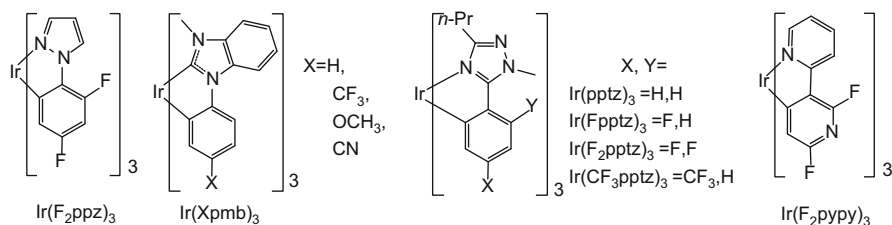
Fig. 11.10 Complexes having characteristic heterocyclic rings

proposed that this was due to the bond weakness between iridium and the ligand nitrogen atoms, and they therefore synthesized a complex with a carbene type ligand [43]. In 2010, we examined the substituent effect of the tris(1-phenyl-3-methylbenzimidazolin-2-ylidene) iridium (III) (Ir(pmb)₃). *fac*-Ir(CF₃pmb)₃ and *fac*-Ir(CH₃Opmb)₃ exhibited deep blue phosphorescence with λ_{max} at 396 and 403 nm ($\Phi_{PL} = 0.84$ and 0.76), respectively (Fig. 11.10) [15]. *fac*-Ir(pmb)₃ had poor solubility, which was improved to some extent using *N*-butyl substitution. However, there are no appropriate host and charge carrier materials for such large band gap complexes; therefore, the external quantum efficiency of the OLED device was only 2.6 % [55].

Samuel and co-workers reported a series of phenyl triazole type complexes in 2006 [56]. The *fac*-iridium (III) tris(1-methyl-5-phenyl-3-propyl-[1,2 4] triazolate) (Ir(pptz)₃ in Fig. 11.10), *fac*-iridium (III) tris(1-methyl-3-propyl-5-(4-fluorophenyl)-1*H*-[1,2,4]triazolate) (Ir(Fpptz)₃), and *fac*-iridium (III) tris (1-methyl-3-propyl-5-(4,6-difluorophenyl)-1*H*-[1,2,4]triazolate) (Ir(F₂pptz)₃) complexes had λ_{max} at 449 ($\Phi_{PL} = 0.66$), 428 ($\Phi_{PL} = 0.27$), and 425 nm ($\Phi_{PL} = 0.03$), respectively. Φ_{PL} decreased by the increase of the number of substituted fluorine atoms; however, it is interesting that the chromaticity coordinate of Ir(pptz)₃ (0.16, 0.20) was deeper than the device composed of FIr6 (0.16, 0.26).

In 2009, Kang and co-workers reported that the phenyl ring of phenyl-pyridine was also converted to a heterocycle. *fac*-tris(2′,6′-difluoro-2,3′-bipyridinato-*N,C⁴′*) iridium(III) (*fac*-Ir(F₂pypy)₃) exhibited λ_{max} at 438 nm ($\Phi_{PL} = 0.71$) [57].

Research on blue phosphorescent iridium complexes is currently performed based on approaches (1)–(3). Complex that have generally high efficiency have long emission lifetimes that are inadequate for device fabrication [45], and complexes with λ_{max} shorter than 450 nm have very small quantum efficiency (for example complex Ir(F₂pptz)₃).

There have been reports of complexes having phenylpyrazole and phenyltriazole type ligands; however, only a few reports of phenylimidazole derivatives. In 2009, Grätzel and co-workers reported a diketonate complex, iridium (III) bis(1-methyl-2-phenylimidazolato)acetylacetonate (N966) [58], which gives a broad emission between 440 and 800 nm that is applicable to a single molecular white lighting OLED.
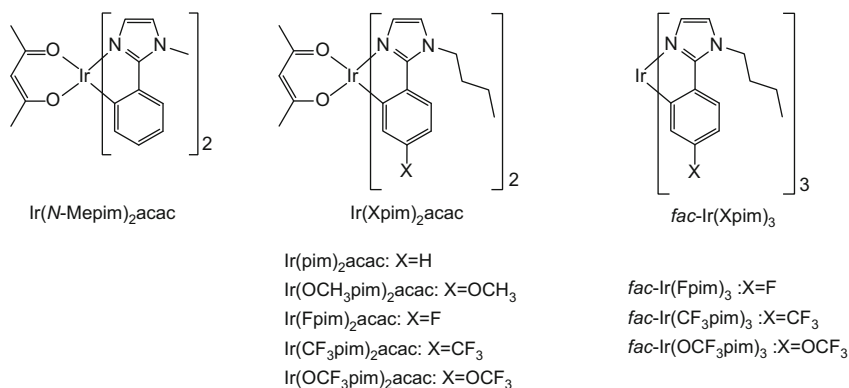
Ir(*N*-Mepim)₂acac   Ir(Xpim)₂acac   *fac*-Ir(Xpim)₃

Ir(pim)₂acac: X=H
Ir(OCH₃pim)₂acac: X=OCH₃
Ir(Fpim)₂acac: X=F
Ir(CF₃pim)₂acac: X=CF₃
Ir(OCF₃pim)₂acac: X=OCF₃

fac-Ir(Fpim)₃ :X=F
fac-Ir(CF₃pim)₃ :X=CF₃
fac-Ir(OCF₃pim)₃ :X=OCF₃

Fig. 11.11 Homoleptic and heteroleptic phenylimidazolynato complexes

Grätzel and co-workers also reported continuous substituents and ancillary ligand effects for N966 in 2011 [59]. They examined the effect of methyl and phenyl groups as *N*-substituents, and also examined chloro substitution on a phenyl ring. For example, iridium (III) bis(4,5-dimethyl- 1,2-diphenylimidazolato)-4-(dimethylamino)picolinate (Ir(Ph₂pim)₂dmapic) has λ_{max} at 539 nm ($\Phi_{PL} = 0.22$) and iridium (III) bis(4-methyl-1,2,5-triphenylimidazolato)- acetylacetonate (Ir(pmppim)₂acac) has λ_{max} at 551 nm with an efficiency of $\Phi_{PL} = 0.95$. The aim of this research was also to achieve white phosphorescence. In the same year, Perumal and co-workers also reported substituent and solvent effects on the emission of diketonate complexes [60]. For example, iridium(III) bis(4,5-dimethyl-1-(3,5-dimethylphenyl)-2-fluorophenylimidazolato)acetylacetonate (Ir(pmdmpim)₂acac) had a green emission of λ_{max} at 514 nm ($\Phi_{PL} = 0.56$). Both reports of phenylimidazolinato complexes do not deal with the blue phosphor, and there is no report of homoleptic complexes. However, there are some patents of phenylimidazolinato complexes [61–66], such as that applied by Konica–Minolta in 2006 [61].

Phenylimidazolinato complexes are one of the important candidates for blue phosphorescent materials. In particular, we have synthesized phenylimidazolinato complexes with various substituents introduced on the phenyl ring (Fig. 11.11), and examined their effects on the photophysical properties and frontier orbitals (HOMO and LUMO).

MO analysis of *fac*-Ir(ppy)₃ indicated that the HOMO is mainly localized in the d-orbital of iridium atom (46.4–56.0 %) and phenyl moiety (30.7–39.8 %) [56] as shown in Table 11.4. Similar behavior has been observed in *fac*-Ir(ppz)₃[67]. On the other hand, detailed analysis of the MOs of *fac*-Ir(CF₃pim)₃, *fac*-Ir(OCF₃pim)₃, and *fac*-Ir(Fpim)₃ revealed the HOMO contribution of the phenyl moiety was 30.7–32.8 % [16], which is smaller than that of *fac*-Ir(ppy)₃ (38.9 %). Accordingly, the contribution of the imidazole ring part (13.3–15.0 %) is higher than that of the pyridine part (8.2 %) in *fac*-Ir(ppy)₃.

The LUMO localized on the ligand (nearly 100 %) is the same result as that for *fac*-Ir(ppy)₃ [56] and *fac*-Ir(ppz)₃ [67]. These results strongly indicate a

Table 11.4 Calculated contribution of iridium metal (Ir), phenyl (Ph), and heterocyclic (Hetero) moieties to HOMO and LUMO

	HOMO			LUMO		
	Ir	Ph	Hetero[a]	Ir	Ph	Hetero[a]
fac-Ir(ppy)$_3$ [56]	52.8	38.9	8.2	0.2	25.9	73.5
fac-Ir(pmb)$_3$ [43]	30.2	47.7	22.1	2.5	2.5	95
fac-Ir(CF$_3$pmb)$_3$ [15]	40.3	38.5	21.2	3.2	19.7	77.1
fac-Ir(pptz)$_3$ [56]	56.6	31.8	10.7	0	49.2	46.7
fac-Ir(CF$_3$pptz)$_3$ [56]	58.6	30.8	9.7	0.1	56.1	36.8
fac-Ir(Fpim)$_3$ [16]	52.4	32.8	14.8	0.6	53.6	45.8
fac-Ir(CF$_3$pim)$_3$ [16]	56	30.7	13.3	0.4	64.1	35.5
fac-Ir(OCF3pim)$_3$[16]	53.2	31.8	15	0.5	57	42.5

[a]Hetero means heterocyclic moiety, thus, pyridyl, benzoimidazolyl, triazolyl, or imidazolyl group including alkyl substituents on it

HOMO–LUMO transition with MLCT character. Details of the LUMO in the phenyl (Ph) moieties (53.6–64.1 %) of homoleptic *fac*-Ir(CF$_3$pim)$_3$, *fac*-Ir (OCF$_3$pim)$_3$, and *fac*-Ir(Fpim)$_3$ have higher contribution than those of the imidazolyl (Im) parts (35.5–45.8 %) [16]; therefore, these populations are quite different from the LUMO of *fac*-Ir(ppy)$_3$ [56] with 73.5 % pyridyl (Py) and 25.9 % phenyl moieties.

The calculated results indicate that the HOMO of iridium phenylimidazolinate complexes have similar or slightly smaller contributions at the phenyl moiety, as with *fac*-Ir(ppy)$_3$; however, much larger localization of the LUMO at the phenyl moiety. Therefore, substitution of the phenyl group by EWGs affects not only the HOMO, but also the LUMO [16]. This type of HOMO–LUMO relation has also been reported for iridium phenyltriazolinate complexes [56].

The contributions of phenyl ring and heterocyclic ring parts of diketonate complexes were similar to those of *fac*-Ir(ppy)$_3$; however, the contribution of the iridium d-orbital had smaller values 46–48 % and these decreases appeared as increase of acetylacetone parts (4.6–5.8 %). Therefore, in *fac*-Ir(CF$_3$pim)$_3$, *fac*-Ir (OCF$_3$pim)$_3$, and *fac*-Ir(Fpim)$_3$, the substitution of EWGs on the phenyl ring is less effective to stabilize the HOMO than in the case of *fac*-Ir(ppy)$_3$ (Table 11.5) [16].

The LUMO of diketonate complexes also has a higher coefficient at the phenyl moiety (51.2–62.3 %) than at the imidazole moiety (35.7–46.3 %), similar to the homoleptic complexes. However, there are two exceptions, Ir(OCH$_3$pim)$_2$acac and Ir(pim)$_2$acac, where the LUMO is localized at acetylacetone (93.6 and 83.8 %, respectively). In addition to these two extreme cases, other diketonate complexes have a LUMO + 1 (MHacac and Ir(Fpim)$_2$acac) or LUMO + 2 (Ir(CF$_3$pim)$_2$acac and Ir(OCF$_3$pim)$_2$acac) localized at acetylacetone. Complexes with trifluoromethyl substituents, *fac*-Ir(CF$_3$pim)$_3$ and Ir(CF$_3$pim)$_2$acac, have LUMO highly localized at the phenyl moiety with 64.1 and 62.3 %, respectively.

Substitution of the acetylacetonate complex has a significant effect on the emission quantum efficiency. This can be explained from the energy difference (ΔE) between the LUMO and MO localized on the acetylacetone moiety. Table 11.5

Table 11.5 Calculated energy levels of the HOMO, LUMO, LUMO + 1, and LUMO + 2 and contribution of iridium metal (Ir), phenyl (Ph), imidazolyl (Im), and acetylacetonate (acac) moieties [16]

		Ir	Ph	Im	acac	E (eV)
Ir(Fpim)₂acac	LUMO + 2	3.6	42.3	39.7	14.4	0.74
	LUMO + 1	1.4	7.5	7.4	83.7	0.87
	LUMO	2.1	51.9	45.6	0.4	0.88
	HOMO	46.4	38.4	10.2	5.0	4.86
Ir(CF₃pim)₂acac	LUMO + 2	2.2	1.2	1.0	95.6	1.05
	LUMO + 1	2.8	60.3	34.3	2.6	1.41
	LUMO	1.6	62.3	35.7	0.4	1.54
	HOMO	48.8	36.8	8.6	5.8	5.16
Ir(OCF₃pim)₂acac	LUMO + 2	2.8	10.5	8.8	77.9	1.03
	LUMO + 1	2.2	43.0	34.5	20.3	1.15
	LUMO	1.9	55.4	42.3	0.4	1.25
	HOMO	47.6	37.0	9.9	5.5	5.16
Ir(OCH₃pim)₂acac	LUMO + 2	3.0	46.4	46.2	4.4	0.31
	LUMO + 1	2.0	50.9	46.8	0.3	0.43
	LUMO	1.6	2.2	2.6	93.6	0.54
	HOMO	46.4	38.9	10.0	4.6	4.43
Ir(pim)₂acac	LUMO + 2	3.6	42.2	39.8	14.4	0.50
	LUMO + 1	2.1	51.7	45.8	0.4	0.64
	LUMO	1.4	7.4	7.4	83.8	0.64
	HOMO	47.0	39.8	8.4	4.8	4.48

shows the percentage MO (LUMO to LUMO + 2) contribution of iridium metal (Ir), phenyl (Ph), imidazolyl (Im), and acetylacetonate (acac) moieties, and the MO energy levels (E) calculated by the DFT method. For example, in the case of CF₃acac, ΔE is 0.49 eV (E_{LUMO}–E_{LUMO+2} = 1.54–1.05), and for OCF₃acac, ΔE is 0.22 eV (E_{LUMO}–E_{LUMO+2} = 1.25–1.03). This indicates that a larger ΔE gives a larger Φ_{PL}; therefore, simple MO energy levels calculated for optimized structure are useful to understand nonradiative deactivation processes through the ancillary ligand. The weak and broad emission of Ir(CF₃pim)₂acac and Ir(OCF₃pim)₂acac at 298 K is caused by the quenching of excitation energy by the acetylacetone part. The inefficiencies of other diketonated complexes at 298 K are due to thermal activation to the upper excited state responsible for nonradiative deactivation. Therefore, these thermal activations are prohibited at 77 K. The smallest Φ_{PL} of Ir(OCH₃pim)₂acac and Ir(pim)₃acac among the diketonate complexes at 77 K is explained by the LUMO being localized on acetylacetone [16].

In contrast, the homoleptic complexes showed efficient emission, not only at 77 K, but also at 298 K (Φ_{PL} = 0.40–0.60). No significant difference of k_r between the homoleptic and diketonate complexes was evident, whereas k_{nr} become smaller for the homoleptic complexes than for the diketonate complexes. For example, in the case of *fac*-Ir(Fpim)₃ and Ir(Fpim)₂acac, k_r is almost the same (1.1 and 1.7×10^5 s⁻¹); however, k_{nr} decreased by almost 1/300.

OLED devices were fabricated for fac-Ir(OCF$_3$pim)$_3$, which showed efficient luminescence in 2MeTHF, and FIrpic was used as a reference. Device was composed of ITO/PEDOT: PSS/mB-4Cz/BCP/CsF/Al. The wet-processable m-terphenyl derivative, 3,3″,5,5″-tetra(9H-carbazol-9-yl)-1,1′:3′,1″-terphenyl (mB-4Cz), was synthesized and used as a host material [17, 68]. The performance of the fabricated devices were determined from plots of current density (J: mA/cm^2), luminance (L: cd/m^2), and current efficiency (η: cd/A) versus applied voltage (V: V).

EL spectra of both devices were red-shifted by 2–3 nm and had smaller 0–0 bands than the 0–1 band, compared with the spectra measured in 2MeTHF. Therefore, the CIE coordinates (x and y) were slightly increased; the coordinate of FIrpic is more blue than fac-Ir(OCF$_3$pim)$_3$; however, there was no significant difference observed by visual check.

The maximum luminance for fac-Ir(OCF$_3$pim)$_3$ and FIrpic was 889 and 3,490 cd/m^2, respectively. The lower luminance of fac-Ir(OCF$_3$pim)$_3$ is explained by inefficient carrier injection into the emitting layer. This is supported by both the inefficient current density and larger driving voltage. The HOMO–LUMO energy levels of fac-Ir(OCF$_3$pim)$_3$ were shifted by approximately 0.7 eV to higher energy than those for FIrpic.

From the energy diagram, the HOMO–LUMO level of fac-Ir(OCF$_3$pim)$_3$ is moved by 0.7 V almost parallel to those of FIrpic in the anodic direction. Therefore, charge injection from the charge conducting layer to the emitting layer became difficult in the case of fac-Ir(OCF$_3$pim)$_3$. The HOMO level of fac-Ir(OCF$_3$pim)$_3$ is higher than that of PEDOT:PSS. The HOMO–LUMO energy levels of imidazole have been reported to take high values among some nitrogen-containing cyclic compounds, according to ab initio calculations [69].

The FIrpic device has the same configuration with the mB-4Cz host materials. A hole only device (device fabricated without a PEDOT: PSS layer) and an electron only device (device fabricated with no BCP layer) were fabricated and the J-V characteristics were measured. The hole and electron only devices showed current densities of 237 and 64 mA/cm^2, respectively, at an applied voltage of 10 V [68]. Therefore, the high hole and low electron transferability of mB-4Cz is partly responsible for the moderate performance of these devices.

11.4 Wet Processable Host Materials for Phosphorescent OLED

Importance of the materials for PHOLED is directly affected to the performance of the devices, as I already mentioned in earlier section. In addition, host materials and device fabrication process has been caught attentions. Because of their high quantum efficiency and low-cost processing, considerable research has been made on solution processable materials for PHOLED during the last decade [70–78].

However, most of these solution processable materials for PHOLED are based on the polymer materials, which have an inherent number of problems, including lower carrier mobility of host materials, shorter lifetime of EL devices, especially their difficult syntheses and purifications [78, 79]. Recently, soluble small molecule-based PHOLEDs have been reported [78–85], which can be overcoming above problems of polymer hosts. On the other hand, because of their high triplet energy gap and bipolar nature of carrier transport, carbazole units frequently have been used in phosphorescence host materials. For example, 4,4′-bis(9-carbazolyl)-2,2′-biphenyl (CBP), 1,4-di(9H-carbazolyl)benzene (CCP) [86], 4,4′-N-N′-dicarbazoleterphenyl (CTP) [87], 1,3-bis(9-carbazolyl)benzene (mCP) [88], and 2,2′- di(9H-carbazole-9-yl)biphenyl (o-CBP) [89]. These small-molecule hosts could be great host materials in vacuum deposited device, however not be obtained approving EL performance in solution processed device. This is because these small-molecule hosts possess the lower glass transition temperature (T_g), lead to the occurrence of crystallization upon drying of emitting layer, thus cannot form a uniform amorphous thin film [80]. Therefore, to obtain better performance of EL device great needs to increase the T_g for small-molecular hosts in solution processed device.

It is conceivable that above carbazole-based hosts can be easily used to solution process through the relatively simple molecular design. Along this respect, in this paper, we report two small-molecule host materials for solution processing PHOLED, 1,4-bis(3,6-di([1,1′:3′,1″:3″,1‴:3‴,1⁗-quinquephenyl]-5″-yl)-9H-carbazol-9-yl)benzene (P-mPCCP) and 1,4-bis(3,6-bis(4,4″-di-tert-butyl-[1,1′:3′,1-″-terphenyl]-5′-yl)-9H-carbazol-9-yl) benzene (T-mPCCP) (Fig. 11.12). We have
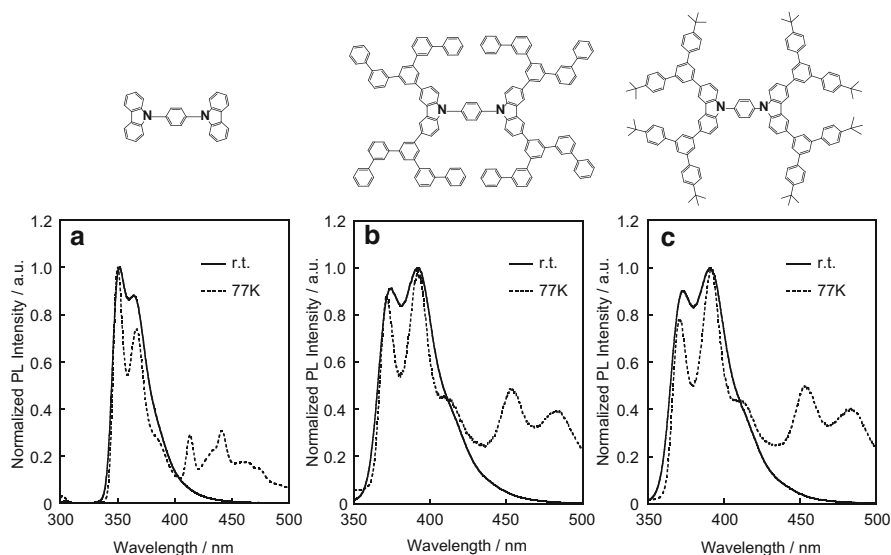

Fig. 11.12 Molecular structures (*above*) and (**a**) PL spectra of CCP, (**b**) P-mPCCP, and (**c**) T-mPCCP at room temperature (*solid line*) and 77 K in Me-THF (*dotted line*)

chosen the CCP as the molecular core because of its good solubility and high triplet energy relative to order carbazol-based hosts, such as well-known CBP. In order to advance thermal stability of host materials, the *m*-terphenyl group attached to the CCP molecule. Since possessing of high E_T and high carrier mobility, *m*-terphenyl group has been successfully applied to phosphorescent host designing [78, 90, 91]. However, combining with *m*-terphenyl group generally molecules become very rigid and difficult to dissolve in common organic solvents. Actually, host material, 1,4-bis(3,6-bis([1,1′:3′,1″-terphenyl]-5′-yl)-9*H*-carbazol-9-yl)benzene (mPCCP) synthesized in this study was also insoluble in any solvent used. To improve the solubility, the both approach of increasing of molecular free volume and introduction of *tert*-butyl group was adopted to synthesized P-mPCCP and T-mPCCP, respectively [17].

P-mPCCP and T-mPCCP were prepared as described below. First, compound 5″-bromo-1,1′:3′,1″:3″,1‴:3‴,1‴′-quinquephenyl was prepared from 3-biphenylboronic acid and 1,3,5-tribromobenzene by Pd(PPh$_3$)$_4$ in THF, which then converted to the arylboronic ester of 2-([1,1′:3′,1″:3″,1‴:3‴,1″-″-quinquephenyl]-5″-yl)-4,4,5,5-tetramethyl-1,3,2-dioxaborolane (M1). The same procedure for compound M2 was applied to give compound 2-(4,4″-di-*tert*-butyl-[1,1′:3′,1″-terphenyl]-5′-yl)-4,4,5,5-tetramethyl-1,3,2-dioxaborolane (M2). Next, the Suzuki cross-coupling reaction of compound M1 and compound M2 with 1,4-bis(3,6-diiodo-9*H*- carbazolyl)benzene [92] led to P-mPCCP and T-mPCCP, respectively. The model compound mPCCP was synthesized from CCP and m-terphenyl group. The chemical structures were characterized by ^{1}H NMR, ^{13}C NMR and elemental analysis.
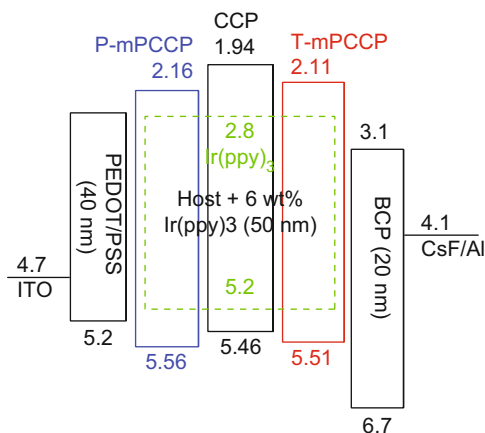
mPCCP showed poor solubility and not soluble in any solvents. Contrast to mPCCP, P-mPCCP and T-mPCCP can readily dissolve in common organic solvents, such as chloroform, 1,2-dichloroethane, toluene, chlorobenzene. For P-mPCCP molecule, although without alkyl group also showed good solubility due to increasing of molecular free volume through additional aromatic ring.

The thermal properties of both compared are evaluated by differential scanning calorimetry (DSC, SII, extar 600). P-mPCCP and T-mPCCP possess high T_g of 161 and 185 °C, respectively, which is significantly higher than the commonly used host materials of CBP (66 °C) and mCP (60 °C). The morphologies of P-mPCCP and T-mPCCP were characterized by AFM (SII, SPA-400). For P-mPCCP and T-mPCCP films doped with 6 wt% Ir(ppy)$_3$, the root-mean square (RMS) values are 0.57 and 0.48 nm, respectively. This indicates that allowing both form morphologically stable and uniform amorphous films in solution process.

P-mPCCP and T-mPCCP have a similar absorption and emission spectra in chloroform and film state, the maximum absorption and emission peak at around 260 and 395 nm, respectively. The absorption band gap was 3.40 eV from the onset of optical absorption in both compounds, which is 0.1 eV lower than that of CCP. The emission spectrum at 77 K is also measured for estimation of the triplet energy (Fig. 11.12). The spectra show the first phosphorescence peak at 452 nm in P-mPCCP and T-mPCCP, corresponding to a triplet energy of 2.70 eV, which is higher than the triplet energy of *fac*-Ir(ppy)$_3$, $E_T = 2.41$ eV [93]. This indicates that

Table 11.6 Physical properties of hosts molecules

Compounds	T_g (°C)	UV–vis/nm	$PL_{\lambda max}$/nm	HOMO[a]/eV	LUMO[b]/eV	ΔE[c]/eV	E_T[d]/eV
CCP	–	293	378	−5.46	−1.94	3.52	3
P-mPCCP	161	254	397	−5.56	−2.16	3.4	2.7
T-mPCCP	185	260	395	−5.51	−2.11	3.4	2.7

[a]HOMO is derived from electrochemical oxidation potentials
[b]LUMO = HOMO + ΔE
[c]ΔE is obtained from the absorption band gap
[d]E_T values estimated from phosphorescence 0,0 band in Fig. 11.12

Fig. 11.13 Energy level diagram for OLED devices

allowing P-mPCCP and T-mPCCP to serve as appropriate host for Ir(ppy)₃. The triplet energy of CCP is calculated to be 3.0 eV, which is 0.3 eV higher than that of P-mPCCP and T-mPCCP. This is because the addition of aromatic ring at 3 or 6 position of carbazole will significantly reduced the triplet energy by expanded the π-electrons of delocalization [94]. The performance of photophysical properties are summarized in Table 11.6.

The electrochemical oxidation potentials of P-mPCCP and T-mPCCP were measured at 0.76 and 0.71 V vs ferrocene/ferricinium ion in CH₂Cl₂; thus, using ferrocene ionization potential of −4.8 eV led to HOMO energy levels of P-mPCCP and T-mPCCP to be −5.56 and −5.51 eV, respectively. We can be deduced that the favorable hole injection from the PEDOT: PSS layer to the emitting layer in EL device. The LUMO energy levels were calculated from HOMO levels and optical band gaps obtained from their absorption spectra to be −2.16 and −2.11 eV, respectively.

To investigate the OLED properties of P-mPCCP and T-mPCCP composing devices, EL device with a structure of ITO/PEDOT:PSS (40 nm)/hosts + 6 wt% Ir (ppy)₃ (50 nm)/BCP (20 nm)/CsF (2 nm)/Al (100 nm) was fabricated (Fig. 11.13). As shown in Fig. 11.14a, the EL spectra of both devices are almost similar and showed a maximum emission peak at 510 nm, with the emission of Ir(ppy)₃,
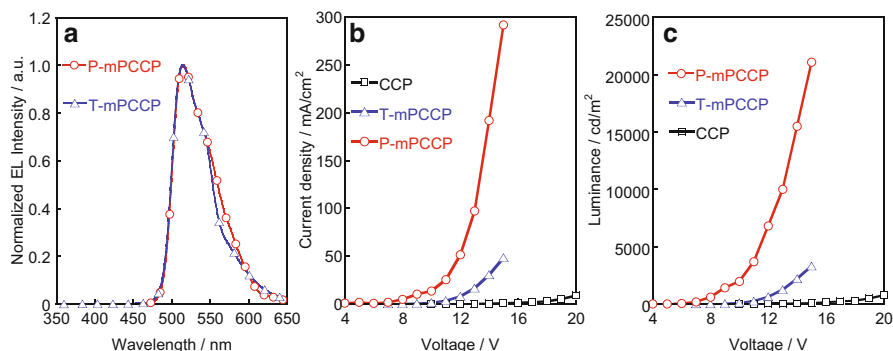
Fig. 11.14 (**a**) EL spectra, (**b**) *I-V* characteristic and (**c**) *L-V* characteristic of OLED devices

without trace of host emission at around 400 nm. The PL spectra of doped $Ir(ppy)_3$ in P-mPCCP and T-mPCCP were similar to their EL spectra and intensities at their maxima had no significant difference. This indicated that an efficient energy transfer occurred from both host to guest $Ir(ppy)_3$. The properties of these devices are compared to that of CCP composing device. The current–voltage (*I-V*) and luminance-voltage (*L-V*) characteristics are showed Fig. 11.14b, c, respectively. The performance of P-mPCCP and T-mPCCP composing device were much higher than that of CCP composing device. The turn-on voltage of P-mPCCP and T-mPCCP composing device was 4.0 and 7.0 eV (corresponding to 1 cd/m^2) and showed a L_{max} of 21,100 and 3,290 cd/m^2 and a maximum luminance efficiency, $\eta_{c, max}$ of 15.0 and 7.6 cd/A, respectively. In contrast, the CCP composing device was turned on at 10.0 V and showed a L_{max} of only 771 cd/m^2 and a $\eta_{c, max}$ of 5.1 cd/A. This is indicated that introducing *m*-terphenyl derivatives of molecular design is very successful for improve the device performance in solution processed device. The device composed of CCP showed very low performance probably because of insufficient smoothness by the spin coating and poor thermal stability of the emitting layer. The device coated with CCP, crystallization phenomenon was found in the next day.

Although both hosts have a same triplet energy, HOMO and LUMO levels, but the P-mPCCP composing device possessed much higher device performance than that of T-mPCCP composing device, which was maximum luminance of sixfold and maximum luminance efficiency of twofold higher than that of T-mPCCP composing device. We attributed to reducing of carrier mobility by introducing a *t*-butyl alkyl in T-mPCCP based on emitting layer. We fabricated the hole transport only device (ITO/PEDOT: PSS/emitting layer/Al) and electron transport only device (ITO/emitting layer/TPBI/LiF/Al) to investigate the conductivity of emitting layer. As a result, P-mPCCP composing device showed higher the current density of hole and electron, especially electron current density was tenfold higher than that of T-mPCCP.

We also fabricated OLED devices by similar method using FIrpic as phosphorescent dopant, however, those devices performance was poor. Considering triplet

energy of FIrpic ($E_T = 2.62$ eV [77]), those devices satisfied triplet energy requirement, however, there is other factors to be solved. One possible factor is that HOMO–LUMO energy levels of FIrpic are 5.72 and 3.07 eV, respectively. Therefore, HOMO energy level of FIrpic is much higher than those of host materials examined. Selection of materials such as dopant and host molecules is somehow requires tailor-made manner.

References

1. K.A. Belmore, R.A. Vanderpool, J.C. Tsai, M.A. Khan, K.M. Nicholas, J. Am. Chem. Soc. **110**, 2004 (1988)
2. K.K.-W. Lo, C.-K. Chung, T.K.-M. Lee, L.-K. Lui, K.H.-K. Tsang, N. Zhu, Inorg. Chem. **42**, 6886 (2003)
3. M.C. DeRosa, D.J. Hodgson, G.D. Enright, B. Dawson, C.E.B. Evans, R.J. Crutchley, J. Am. Chem. Soc. **126**, 7619–7626 (2004)
4. H. Yersin (ed.), *Highly Efficient OLEDs with Phosphorescent Materials* (Wiley VCH, Berlin, 2007)
5. D. Tanaka, H. Sasabe, Y.-J. Li, S.-J. Su, T. Takeda, J. Kido, Jpn. J. Appl. Phys. **46**, L10–L12 (2007)
6. C.W. Tang, S.A. Vanslyke, Appl. Phys. Lett. **51**, 913 (1987)
7. R. Schlaf, B.A. Parkinson, P.A. Lee, K.W. Nebesny, G. Jabbour, B. Kippelen, N. Peyghambarian, N.R. Armstrong, J. Appl. Phys. **84**, 6729–6736 (1998)
8. M.A. Baldo, D.F. O'Brien, Y. You, A. Shoustikov, S. Sibley, M.E. Thompson, S.R. Forrest, Nature **395**, 151 (1998)
9. D.F. O'Brien, M.A. Baldo, M.E. Thompson, S.R. Forrest, Appl. Phys. Lett. **74**, 442 (1999)
10. M.A. Baldo, S. Lamansky, P.E. Burrows, M.E. Thompson, S.R. Forrest, Appl. Phys. Lett. **75**, 4 (1999)
11. M.A. Baldo, M.E. Thompson, S.R. Forrest, Nature **403**, 750 (2000)
12. T. Karatsu, T. Nakamura, S. Yagai, A. Kitamura, K. Yamaguchi, Y. Matsushima, T. Iwata, Y. Hori, T. Hagiwara, Chem. Lett. **32**, 886 (2003)
13. T. Karatsu, E. Ito, S. Yagai, A. Kitamura, Chem. Phys. Lett. **424**, 353 (2006)
14. K. Tsuchiya, E. Ito, S. Yagai, A. Kitamura, T. Karatsu, Eur. J. Inorg. Chem. **2104** (2009)
15. K. Tsuchiya, S. Yagai, A. Kitamura, T. Karatsu, K. Endo, J. Mizukami, S. Akiyama, M. Yabe, Eur. J. Inorg. Chem. 926 (2010)
16. T. Karatsu, M. Takahashi, S. Yagai, A. Kitamura, Inorg. Chem. **52**, 12338 (2013)
17. X. Lin, S. Yagai, A. Kitamura, D.-R. Hwang, S.-Y. Park, Y.-S. Park, J.-J. Kim, T. Karatsu, Synth. Met. **162**, 303 (2012)
18. X. Lin, T. Hattori, S. Yagai, A. Kitamura, T. Karatsu, J. Photopolym. Sci. Tech. **24**, 299 (2011)
19. G. Zhou, W.-Y. Wong, S. Suo, J. Photochem. Photobiol. C Photochem. Rev. **11**(133) (2010)
20. M. Nonoyama, Bull. Chem. Soc. Jpn. **47**, 767 (1974)
21. K.A. King, P.J. Spellane, R.J. Watts, J. Am. Chem. Soc. **107**, 1431 (1985)
22. K. Dedeian, P.I. Djurovich, F.O. Garces, G. Garlson, R.J. Watts, Inorg. Chem. **30**, 1685 (1991)
23. M.G. Colombo, T.C. Brunold, T. Riedener, H.U. Güdel, M. Förtsch, H.-B. Bürgi, Inorg. Chem. **33**, 545 (1994)

24. A.B. Tamayo, B.D. Alleyne, P.I. Djurovich, S. Lamansky, I. Tsyba, N.N. Ho, R. Bau, M.E. Thompson, J. Am. Chem. Soc. **123**, 7377 (2003)
25. V.V. Grushin, N. Herron, D.D. LeCloux, W.J. Marshall, V.A. Petrov, Y. Wang, Chem. Commun. 1494 (2001)
26. J.N. Demas, G.A. Crosby, J. Am. Chem. Soc. **92**, 7262 (1970)
27. J.N. Demas, G.A. Crosby, J. Am. Chem. Soc. **93**, 2841 (1971)
28. R.J. Watts, G.A. Crosby, J. Am. Chem. Soc. **94**, 2606 (1972)
29. R.J. Watts, G.A. Crosby, J.L. Sansregret, Inorg. Chem. **11**, 14 (1972)
30. K. Koike, N. Okoshi, K. Takeuchi, O. Ishitani, H. Tsubaki, I.P. Clark, M.W. George, F.P.A. Johnson, J.J. Turner, J. Am. Chem. Soc. **124**, 11448 (2002)
31. A.W. Adamson, J. Phys. Chem. **71**, 798 (1967)
32. L.G. Vanquickienborne, A. Ceulemans, J. Am. Chem. Soc. **99**, 2208 (1977)
33. L.G. Vanquickienborne, A. Ceulemans, Inorg. Chem. **17**, 2730 (1978)
34. L.G. Vanquickienborne, A. Ceulemans, Coord. Chem. Rev. **48**, 157 (1983)
35. E. Larsen, G.N. La Mar, J. Chem. Educ. **51**, 633 (1974)
36. G.L. Miessler, D.A. Tarr, *Inorganic Chemistry*, 3rd edn. 2004 (Prentice Hall Inc, New Jersey)
37. E.J. Nam, J.H. Kim, B.-O. Kim, S.M. Kim, N.G. Park, Y.S. Kim, Y.K. Kim, Y. Ha, Bull. Chem. Soc. Jpn. **77**, 751 (2004)
38. N. Ide, N. Matsusue, T. Kobayashi, H. Naito, Thin Soild Films **509**, 164 (2006)
39. L. Xiao, Z. Chen, B. Qu, J. Luo, S. Kong, Q. Gong, J. Kido, Adv. Mater. **23**, 926 (2011)
40. C. Adachi, R.C. Kwong, P. Djurovich, V. Adamovich, M.A. Baldo, M.E. Thompson, S.R. Forrest, Appl. Phys. Lett. **79**, 2082 (2001)
41. R.J. Holmes, B.W. D'Andrade, S.R. Forrest, X. Ren, J. Li, M.E. Thompson, Appl. Phys. Lett. **83**, 3818 (2003)
42. S.-J. Yeh, M.-F. Wu, C.-T. Chen, Y.-H. Song, Y. Chi, M.-H. Ho, S.-F. Hsu, C.H. Chen, Adv. Mater. **17**, 285 (2005)
43. T. Sajoto, P.I. Djurovich, A. Tamayo, M. Yousufuddin, R. Bau, M.E. Thompson, R.J. Holmes, S.R. Forrest, Inorg. Chem. **44**, 7992 (2005)
44. V. Sivasubramaniam, F. Brodkorb, S. Hanning, H.P. Loebl, V. van Elsbergen, H. Boerner, U. Scherf, M. Kreyenschmidt, J. Fluor. Chem. **130**, 640 (2009)
45. C.-H. Lin, Y.-Y. Chang, J.-Y. Hung, C.-Y. Lin, Y. Chi, M.-W. Chung, C.-L. Lin, P.-T. Chou, G.-H. Lee, C.-H. Chang, W.-C. Lin, Angew. Chem. Int. Ed. **50**, 3182 (2011)
46. S. Lamansky, P. Djurovich, D. Murphy, F. Abdel-Razzaq, R. Kwong, I. Tsyba, M. Bortz, B. Mui, R. Bau, M.E. Thompson, Inorg. Chem. **40**, 1704 (2001)
47. S. Lamansky, P. Djurovich, D. Murphy, F. Abdel-Razzaq, H.-E. Lee, C. Adachi, P.E. Burrows, S.R. Forrest, M.E. Thompson, J. Am. Chem. Soc. **123**, 4304 (2001)
48. R. Ragni, E.A. Plummer, K. Brunner, J.W. Hofstraat, F. Babudri, G.M. Farinola, F. Naso, L. De Cola, J. Mater. Chem. **16**, 1161 (2006)
49. S. Takizawa, H. Echizen, J. Nishida, T. Tsuzuki, S. Tokito, Y. Yamashita, Chem. Lett. **35**, 748 (2006)
50. M.L. Xu, R. Zhou, G.Y. Wang, Q. Xiao, W.S. Dua, G.B. Che, Inorg. Chim. Acta **361**, 2407 (2008)
51. P. Coppo, E.A. Plummerab, L. De Cola, Chem. Commun. 1774 (2004)
52. C.-H. Yang, Y.-M. Cheng, Y. Chi, C.-J. Hsu, F.-C. Fang, K.-T. Wong, P.-T. Chou, C.-H. Chang, M.-H. Tsai, C.-C. Wu, Angew. Chem. Int. Ed. **46**, 2418 (2007)
53. Y.-C. Chiu, C.-H. Lin, J.-Y. Hung, Y. Chi, Y.-M. Cheng, K.-W. Wang, M.-W. Chung, G.-H. Lee, P.-T. Chou, Inorg. Chem. **48**, 8164 (2009)
54. J.-Y. Hung, Y. Chi, I-H. Pai, Y.-C. Yu, G.-H. Lee, P.-T. Chou, K.-T. Wong, C.-C. Chenc, C.-C. Wu, Dalton Trans., 6472 (2009)
55. R.J. Holmes, S.R. Forrest, T. Sajoto, A. Tamayo, P.I. Djurovich, M.E. Thompson, J. Brooks, Y.-J. Tung, B.W. D'Andrade, M.S. Weaver, R.C. Kwong, J.J. Brown, Appl. Phys. Lett. **87**, 243507 (2005)

56. S.-C. Lo, C.P. Shipley, R.N. Bera, R.E. Harding, A.R. Cowley, P.L. Burn, I.D.W. Samuel, Chem. Mater. **18**, 5119 (2006)
57. S.J. Lee, K.-M. Park, K. Yang, Y. Kang, Inorg. Chem. **48**, 1030 (2009)
58. H.J. Bolink, F. De Angelis, E. Baranoff, C. Klein, S. Fantacci, E. Coronado, M. Sessolo, K. Kalyanasundaram, M. Graetzel, Md. K. Nazeeruddin, Chem. Commun. 4672 (2009)
59. E. Baranoff, S. Fantacci, F. De Angelis, X. Zhang, R. Scopelliti, M. Graetzel, M.K. Nazeeruddin, Inorg. Chem. **50**, 451–462 (2011)
60. J. Jayabharathi, V. Thanikachalam, N. Srinivasan, M.V. Perumal, J. Fluoresc. **21**, 1585–1597 (2011)
61. T. Oshiyama, M. Nishizeki, N. Sekine, H. Kita, Japan Patent, P2006-60198A (2006)
62. J. Adler, A. Kanitz, G. Schmid, O. Freydenzon, A. Maltenberger, U.S. Patent, US2010/0213824 A1 (2010)
63. O. Molt, C. Lennartz, K. Dormann, E. Fuchs, T. Geβner, N. Langer, S. Watanabe, C. Schildknecht, G. Wagenblast, U.S. Patent, US2010/0253988 A1 (2010)
64. C.-H. Cheng, W.-H. Liao, H.-H. Shih, M.-J. Huang, T.-W. Tang, U.S. Patent, US 8,062,767 B2 (2011)
65. F. Okuda, T. Iwakuma, K. Yamamichi, C. Hosokawa, U.S. Patent, US 2011/0017984 A1 (2011)
66. S. Otsu, M. Nishizeki, E. Katoh, T. Oshiyama, U.S. Patent, US 2011/0073851 (2011)
67. T. Fei, X. Gu, M. Zhang, C. Wang, M. Hanif, H. Zhang, Y. Ma, Synth. Met. **159**, 113 (2009)
68. T. Hattori, Master Thesis, Chiba University, 2012
69. K. Tamao, M. Uchida, T. Izumizawa, K. Furukawa, S. Yamaguchi, J. Am. Chem. Soc. **118**, 11974 (1996)
70. X.W. Chen, J.L. Liao, S.A. Chen, J. Am. Chem. Soc. **125**, 636 (2002)
71. S. Tokito, M. Suzuki, F. Sato, Org. Electron. **4**, 105 (2003)
72. A.V. Dijken, J.J.A.M. Bastiaansen, K. Brunner, J. Am. Chem. Soc. **126**, 7718 (2004)
73. X.H. Yang, D.C. Muller, K. Meerholz, Adv. Mater. **18**, 948 (2006)
74. Y.C. Chen, G.S. Huang, S.A. Chen, J. Am. Chem. Soc. **128**, 8549 (2006)
75. Y.M. You, S.H. Kim, S.Y. Park, Macromolecules **39**, 349 (2006)
76. S.P. Huang, T.H. Jen, S.A. Chen, J. Am. Chem. Soc. **130**, 4699 (2008)
77. Z.L. Wu, Y. Xiong, Y. Cao, Adv. Mater. **20**, 2359 (2008)
78. W. Jiang, L. Duan, Y. Qiu, J. Mater. Chem. **20**, 6131 (2010)
79. K.S. Yook, S.E. Jang, J.Y. Lee, Adv. Mater. **22**, 4479 (2010)
80. J.H. Jou, W.B. Wang, J. Mater. Chem. **20**, 8411 (2010)
81. Z.Y. Ge, T. Hayakawa, M. Kakimoto, Chem. Mater. **20**, 2532 (2008)
82. Y.T. Tao, Q. Wang, D.G. Ma, J. Mater. Chem. **18**, 4091 (2008)
83. J.Q. Ding, B.H. Zhang, L.X. Wang, Adv. Mater. **21**, 4983 (2009)
84. J.J. Park, T.J. Park, J.H. Kwon, Org. Electron. **10**, 189 (2009)
85. W. Jiang, L. Duan, Y. Qiu, J. Mater. Chem. **21**, 4918 (2011)
86. D.K. Rayabarapu, J.P. Duan, C.H. Cheng, Adv. Mater. **17**, 349 (2005)
87. J.Y. Jeon, T.J. Park, J.Y. Lee, Chem. Lett. **36**, 1156 (2007)
88. R.J. Holmes, S.R. Forrest, M.E. Thompson, Appl. Phys. Lett. **82**, 2422 (2003)
89. J. He, H.M. Liu, D.G. Ma, J. Phys. Chem. C **113**, 6761 (2009)
90. S.C. Lo, G.J. Richards, P.L. Burn, Adv. Funct. Mater. **15**, 1451 (2005)
91. H. Sasabe, Y.J. Pu, J. Kido, Chem. Commun. **19**, 6655 (2009)
92. Q. Zhang, J.S. Chen, L.X. Wang, J. Mater. Chem. **14**, 895 (2004)
93. J.X. Jing, C.Y. Jiang, Y. Cao, Macromolecules **38**, 4072 (2005)
94. K. Brunner, A.V. Dijken, B.M.W. Langeveld, J. Am. Chem. Soc. **126**, 6035 (2004)